Egypt. J. Chem. **Vol. 66** No. 11 pp. 363 - 372 (2023)

Egyptian Journal of Chemistry

http://ejchem.journals.ekb.eg/

Structural, Optical, and Shielding Studies of Some Sb Glasses based Egyptian nano-Rock Wool

Sahar A. El-Gharbawy[1,2*], H. A. Saudi[1], Mohamed Shaban[3,4], M. A. Farag[5], M.Y. Hassaan[5]

[1]Department of Physics, Faculty of Science, Al-Azhar University (Girls' Branch), Nasr City, 11884 Cairo, Egypt.
[2]Housing and Building National Research Center, 87 El-Tahrir St., Dokki, Giza 1770, Egypt.
[3]Nanophotonics and Applications (NPA) Lab, Department of Physics, Faculty of Science, Beni-Suef University, Beni-Suef 62514, Egypt.
[4] Physics Department, Faculty of Science, Islamic University of Madinah, P.O. Box 170, Al Madinah Al Monawara 42351, Saudi Arabia.
[5]Department of Physics, Faculty of Science, Al-Azhar University, Nasr City, 11884 Cairo, Egypt.

Abstract

By the melt quenching process, glass samples with the mol% composition [45 Na_2CO_3 30 B_2O_3 25 nano-Rock wool x Sb_2O_3, $0 \leq x \leq 8$] were produced. X-ray diffraction (XRD), density, molar volume, and infrared spectroscopy were used to analyze the structure of the produced samples. To examine the prepared glasses by UV–visible spectral distributions the samples were measured between 250 and 850 nm. Allowable indirect transitions were discovered using optical absorption data. The energy values of Urbach (Eu) range from 0.35 to 0.24 eV were obtained from prepared samples. It was found that Sb_2O_3 concentration affects all optical characteristics. Using WinXCom software, the mass attenuation coefficient, μ_m, was calculated for the energy range of 0.01 MeV to 20 MeV. The effective atomic numbers, (Z_{eff}), half value layers, (HVL), and mean free path, (MFP) were calculated using the mass attenuation coefficients. The macroscopic effective elimination cross-section for fast neutron ($\sum R$) values was also determined. According to the findings, the investigated glasses were found suitable and promising for optical fiber, optoelectronics, and radiation shielding.

Keywords : Glass, Rockwool, Optical properties, Radiation shielding, Antimony

1. Introduction

Egyptian Rock Wool is mostly silicon oxide, with smaller quantities of aluminum, calcium, iron, magnesium, sodium, and potassium oxides. Rock wool particles are inorganic, biologically inert materials created from bazalting rocks [1]. Rock wool has strong mechanical qualities as well as outstanding stability, and its open cell structure prevents thermal expansion and contraction. Steam may readily travel through the air pockets, which have great thermal conductivity. Because of its short length, Rock Wool may be used to create high-density products with significantly better load-carrying capability than other materials. The glass Rock Wool absorbs sound wave energy owing to cross fibers and air pockets. Rock wool glass is one of the greatest sound absorption insulators for industrial and construction applications because of its structure. Rock wool can be used to reduce vibrations induced by sources such as traffic, ventilation systems, and heavy machinery, in addition to its low weight. Glass wool can resist temperatures up to 750 degrees Celsius. Even when temperatures reach above 900 ° C, as in the case of a fire, Rock Wool preserves its thermal conductivity and capacity to defend against fire. As a result, they must be put in fire protection applications in such a way that they maintain their position and form even after the binder has evaporated owing to fire[2].

*Corresponding author e-mail: fouads5649@gmail.com
Receive Date: 24 August 2022, Revise Date: 04 September 2022, Accept Date: 05 September 2022
DOI: 10.21608/EJCHEM.2022.158253.6845

Thermal conductivity changes according to the temperature of the insulated element. Rock wool has a thermal conductivity of approximately 0,035 and 0,040 W/mK at typical temperatures. The benefit of Rock Wool over other insulating materials is that it maintains its qualities for a long time, even in the event of a major fire. This feature keeps other materials behind the Rock wool from overheating or self-igniting[3]. Antimony-based glass has lately been recognized as a viable material for nonlinear optical applications due to the remarkable capacity of the Sb_2O_3-B_2O_3 system to form glass throughout the whole range of concentrations of the elemental component[4]. Glass ceramics based on Sb_2O_3 have a high refractive index and are transparent to far-infrared wavelengths and has strong density, big transmission window, low phonon energy, low melting and glass transition temperatures, and high linear thermal expansion are all predicted to be characteristics of Sb_2O_3 containing glasses [5]. Antimony oxide may be seen as a tetrahedron with the oxygens at three corners and the lone pair of antimony electrons (Sb^{3+}) at the fourth corner localized in the third equatorial direction of the Sb atom in the glass network with SbO_3 structural units[6]. Antimony ions can exist in the Sb^{5+} state, participate in the formation of a glass network with $Sb^{5+}O_4$ structural units, and form linkages with BO_4 structural units in the $PbO–Sb_2O_3–B_2O_3$ glass ceramic network, all of which can have a significant impact on the nonlinear optical effects of these glass ceramics[6]. Glass is one of the important shielding materials used in the field of nuclear radiation. **[Mehmet Erdem, et al., (2010)]** [7] produced a novel shielding material by a metallurgical solid waste containing lead was analyzed as shielding material for gamma radiation. The photon mass attenuation coefficients (μ/ρ) were measured and calculated using WinXCom computer code for the novel shielding material, concrete and lead. **[Gaber F. A., et al., (2013)]** [8]studied the use of Boron Oxide Glass/Epoxy Ilmenite assembly as a two-layer shield for fast neutrons and gamma ray. They found that the transmitted flux intensity decreases with the increasing of fast neutrons and gamma rays energy for the homogeneous shields and all assemblies. **[A. M. Reda and A. A. El-Daly, (2020)]** [9] studied the shielding parameters of Sn-20Bi (SB) and Sn-20Bi-0.4Cu (SBC) lead-free alloys solidified with and without the effect of a rotating magnetic field (RMF). They illusturated that the results of the shielding parameters confirm that these alloys are good shielding materials against gamma rays.

The goal of this study is to make some Rock Wool glasses, and their amorphous nature will be proven first using XRD. Then look at the UV-visible and infrared spectra of Rock Wool glasses. In this study, half value layer and MFP parameters are investigated in addition to linear and mass attenuation coefficients to recognize the capability of its applications.

2. Experimental Procedure

Gray Fresh Rock wool (RW) samples were delivered from Al Alamia for Rock Wool & Insulations Factory (Rockal), Al-Sharkia, Egypt. The findings of the X-ray fluorescence analysis of the utilized Rock Wool utilizing PANalytical Axios advanced-Netherlands are shown in Table 1. The nano Rock Wool was obtained by ball milling for 24 h at 350 rpm using a ball mill (RETSCH Planetary Ball Mill PM 400, Germany) apparatus free from contaminations [10]. The suggested percentage molecular composition was [45 Na_2CO_3 30 B_2O_3 25 nano-Rock Wool x Sb_2O_3, x = (0, 2, 4, 6, 8)]. To ensure complete mixing, the glass batches were milled for two hours. To achieve homogenous glasses, the acquired combined powders were heated in porcelain crucibles at 1150 ^oC for 2 hours with stirring many times during melting. The melts were then quenched in air between two copper plates, and visual inspection of the resulting glasses revealed that they have the amorphous state. Using the Archimedes technique and toluene as an immersion liquid, the experimental density (ρ_{exp}) of the resulting solid glasses was determined using equation (1),

$$\rho_{\exp} = \frac{M_a}{M_a - M_t}\ \rho_t \qquad (1)$$

where $\boldsymbol{\rho_t}$ is the density of toluene, $\boldsymbol{M_a}$ and $\boldsymbol{M_t}$ of the masses of a sample were in air on in toluene respectively. The empirical density ($\boldsymbol{\rho_{emp}}$) values of the corresponding close packed structure were also calculated by applying equation (2),

$$\rho_{emp} = \sum X_i \rho_i \qquad (2)$$

where $\boldsymbol{\rho_i}$, is the total of the densities of the oxides forming each glass sample, and $\boldsymbol{X_i}$ is the mole fraction of each oxide.

Equation (3) mixing was then used to determine the molar volume ($(V_m)_{exp}$) values. The resulting powder mixtures were [12, 13],

$$(V_m)_{\exp} = \sum (M_i / \rho_{\exp}) \qquad (3)$$

where M_i is the main molecular weight of a sample in (g/mol). The empirical molar volume values were then calculated using equation (3), with replacing ($\boldsymbol{\rho_{exp}}$) by ($\boldsymbol{\rho_{emp}}$) values[11].

XRD patterns of the studied samples were obtained using Rigaku RINT 2100 diffractometer and cut

radiation, between 2θ from 10° to 80° with an interval and scanning rate of 0.02° and 5° min^{-1}, respectively.

The infrared absorption spectra of glasses were measured at room temperature in the wave number range 400-4000 cm^{-1} by a Fourier Transform computerized infrared spectrometer type, JASCO, FT/IR-430, Japan. The samples were investigated as fine powder which was mixed with KBr in the ratio (2:200 mg glass powder to KBr, respectively). The weighed mixture was then subjected to a pressure of 5 tons/cm^2 to produce clear homogeneous discs. The optical absorption of highly polished samples of the studied glasses were recorded at room temperature using a spectrometer in the range 200-1000 nm type JASCO. Corp., V-570, Rel-00, Japan.

Table 1: Chemical analysis of the used Rock Wool

Constituting oxide	**SiO_2**	**CaO**	**Al_2O_3**	**Fe_2O_3**	**MgO**	**Na_2O**	**TiO_2**	**K_2O**	**MnO**
mol (%)	**44.9**	**17.8**	**13.1**	**8.8**	**8.5**	**1.9**	**1.8**	**1.2**	**0.3**

Using WinXCom software, the mass attenuation coefficient, μ_m, was calculated for the energy range of 0.01 MeV to 20 MeV and it was given by the density of the material ρ as eq. (4):

$$\mu_m = \mu_t/\rho = \Sigma_i \; w_i \; (\mu_t/\rho)_i \quad (4)$$

where w_i is the fractional weight. The total linear attenuation coefficient (μ) is calculated by multiplying μ_m by the density (ρ).

The mean free path (MFP) is given by the reciprocal of total attenuation coefficient (μ) as calculated by:

$$MFP = 1/\mu \quad (5)$$

The total interaction σ_a of gamma photons with the shielding, is given by:

$$\sigma_a = (\mu_t/\rho)_{mixture}/[N_A \Sigma_i (w_i/A_i)] \quad (6)$$

where N_A and A_i are the Avogadro's number and the atomic weight of the ith constituent element of the mixture, respectively. The total σ_e of the mixture can computed by:

$$\sigma_e = (1/N_A) \; \Sigma_i \; (f_i A_i/z_i) \; (\mu_t/\rho)_i \quad (7)$$

where f_i represents the fractional abundance and Z_i represents the atomic number of the ith element in a mixture. The atomic number Z of elements of the mixture or compound (Z_{eff}) is calculated by:

$$Z_{eff} = \sigma_a/\sigma_e \quad (8)$$

The N_{eff} (electrons per gram) of the material can be gotten by the equation:

$$N_{eff} = (\mu_t/\rho)_{mixture} / \sigma_e = Z_{eff} \; [N_A \Sigma_i (w_i/A_i)] \quad (9)$$

The neutron disappears inside the shielding material as a result of absorption or elastic and inelastic scattering. The probability of these processes is expressed by the total microscopic cross-section (σ_t) as:

$$\sigma_t = \sigma_s + \sigma_a \quad (10)$$

where σ_s is the scattering cross-section and σ_a is the absorption cross-section. The equivalent atomic number Z_{eq} for particular material has been calculated by matching the ratio $[(\mu/\rho)_{Compton}/(\mu/\rho)_{Total}]$ of that material at a specific energy with the corresponding ratio of an element at the same energy. Half Value Layer (HVL) is the thickness of a shield that reduces the radiation level by a factor of 2 that is to half the initial level [i.e. HVL = ln 2 μ = 0.693 μ][12].

The neutron macroscopic cross-section (Σ_t), which represents the product of the total microscopic cross-section (σ_t) with the number of nuclei per unit volume of the shielding material (N) as in the following equation[13]:

$$\Sigma_t = N \; \sigma_t = \sigma_s + \sigma_a \quad (11)$$

The effective removal cross-section(Σ_R) instead of (Σ_t) for fast neutrons is given by empirical equations:

$$\Sigma_R = \Sigma_i \; W_i \; (\Sigma_R / \rho)_i \quad \&$$

W_i: Partial density (g / cm^3) (12)

3. Result and discussion

3.1. Density and molar volume

The density of the investigated glasses was determined experimentally using the liquid displacement technique, and the results were compared to theoretical values for the close packed structure of the respective compositions. The glassy nature of the produced samples was confirmed by this comparison. For comparison, the experimental and empirical densities were displayed as a function of Sb_2O_3 concentration in Fig. 1. With increasing Sb_2O_3 content, the experimental density and empirical density values increased gradually and linearly. The empirical density is frequently greater than the equivalent experimental density, with experimental density values ranging from [2.477-3.35 (g/cm^3)] and theoretical density values ranging from [2.95-3.83 (g/cm^3)]. On the other hand, since the molar volume is directly related to the internal spatial structure of materials, it is suitable to also consider the molar volume values of the studied glasses[11], and Fig (2) exhibits the wide difference of the obtained molar volume values (empirical and experimental). It shows linear gradual increase as a function of Sb_2O_3 content, and the empirical values appeared usually lower than those obtained experimentally. The experimental molar volume values lie between [25.64- 26.72 (cm^3/mol)], while the theoretical molar volume lie between [23.73- 24.37 (cm^3/mol)]. The density and molar volume behavior (both experimental and empirical) are strongly influenced by the Rock Wool and antimony contents. The amorphous nature and short range order of the examined glass samples may be demonstrated by the greater empirical density and smaller empirical molar volume in contrast to the equivalent experimental values [14].

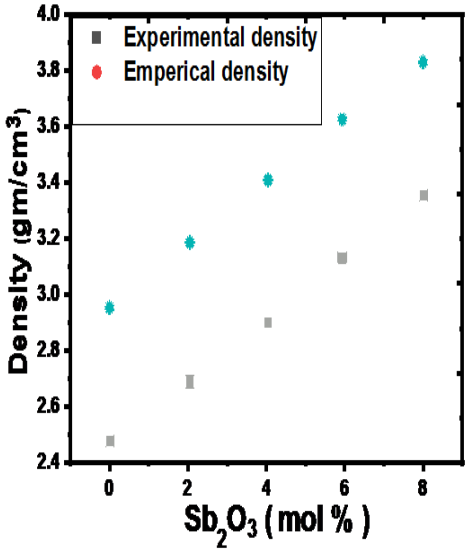

Fig. 1: Experimental and empirical density values as a function of Sb_2O_3 content.

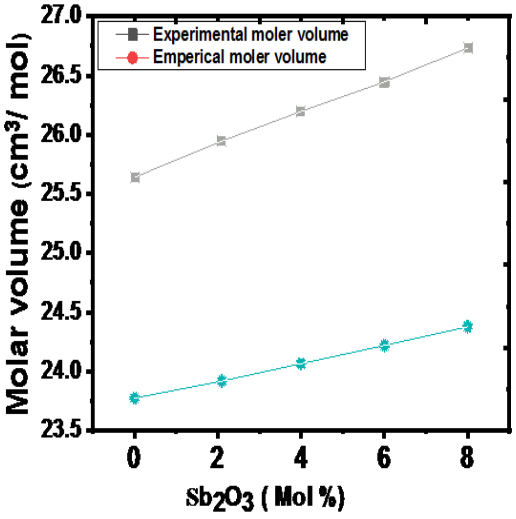

Fig. 2: Experimental and empirical molar volume values as a function of Sb_2O_3 content.

3.2. X-ray diffraction (XRD)

For showing the short-range order of amorphous materials, XRD is currently regarded a required method[15], It was used in this case to confirm the amorphous nature of the prepared samples. In samples x= (4, 6, 8) , the acquired XRD patterns of the examined glasses exhibit two humps around 2θ= 29 degrees with no hint of any diffraction peaks. Fig (3) shows the acquired XRD patterns of samples containing 4, 6, and 8 mol% Sb_2O_3.

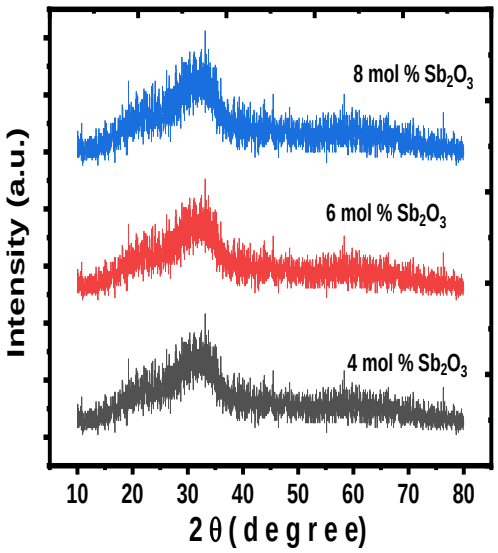

Fig. 3: XRD patterns of the glass samples containing (4, 6 and 8) mol% Sb_2O_3 as represented patterns

3.3 Analysis of absorption edges

Several important optical characteristics may be deduced from the optical absorption edges. These edges are frequently used to compute the optical bandgap energy values for indirect transmissions. E_g is based on the relationship between the optical absorption coefficient (α) and the incident photon energy (hν) (Davis and Mott's equation(4) can be used to compute the optical energy gap[16] .

$$(\alpha h\nu)^{0.5} = B (h\nu \quad (4)$$

where hν is the incident photon energy, B is the band tailing parameter constant, E_g is the optical bandgap energy, and α is the absorption coefficient cm^{-1} calculated using the formula (α = 2.303 × Absorbance/glass thickness) for the present glass system *E_g values* are calculated by extrapolation of the linear sections of the curve of the relationship between $(\alpha h\nu)^{0.5}$ and photon energy hν, as shown in Fig. (4), and then by determining the point of intersection with the horizontal axis. The relation between that obtained E_g values are shown in Fig. (5), which shows a declining trend when Sb_2O_3 is increased. As we will revealed by FTIR results should that as Sb_2O_3 mol% was increased the cation polarization of Sb^{5+} ions by comparison with other ions in the glass matrix increased and caused presence of more non-bridging oxygen ions (NBO's). As a result of the increased disorder within the glass network, the valence band moves to higher energies, and the optical bandgap energy decreased[17]. The existence of short-range regulation in the glass network, referred to the Urbach tail, causes the formation of some protracted

local states in the bandgap[18]. The Urbach energy (E_u) may be used to compute the width of this tail [12], and the current values of Eu can be calculated using the ln(α) and hν relationship, as shown in Fig (6). The inset of Fig. (7) shows that the obtained E_u values growing with the increasing of Sb_2O_3 (mol%). The E_u values ranged from 0.24-0.35 eV, showing that the glasses are semiconductors[19]. On the other hand, The structural stability of the prepared glasses, may be derived from E_u values, with a rise to a value indicating a loss in structural stability [19].

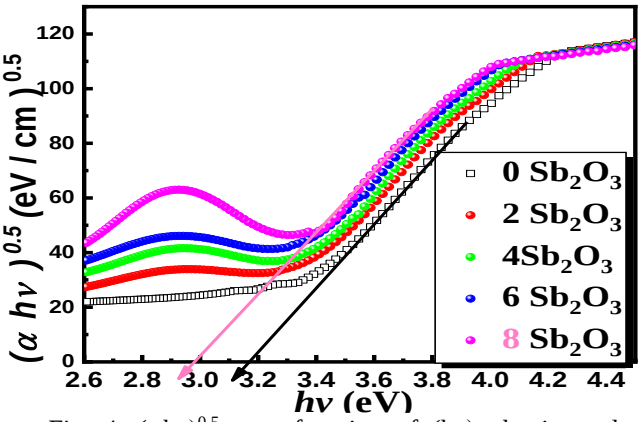

Fig. 4: $(\alpha h\nu)^{0.5}$ as a function of (hν), the inset depicts the evolution of E_g as a variable of Sb_2O_3.

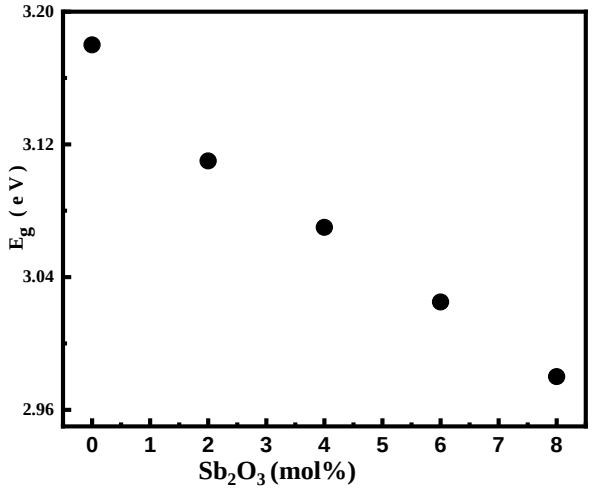

Fig. 5: Indirect optical energy gap E_g as a function of Sb_2O_3 (mol%) of studied glasses.

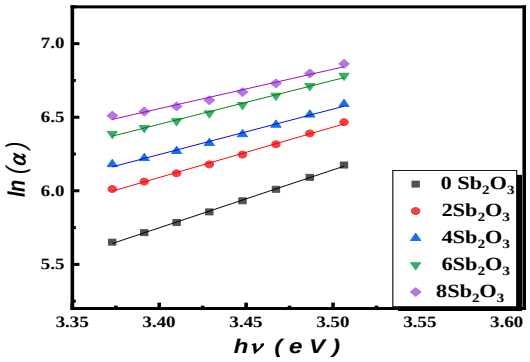

Fig. 6: ln(α) as a function of (hν) of the prepared glasses.

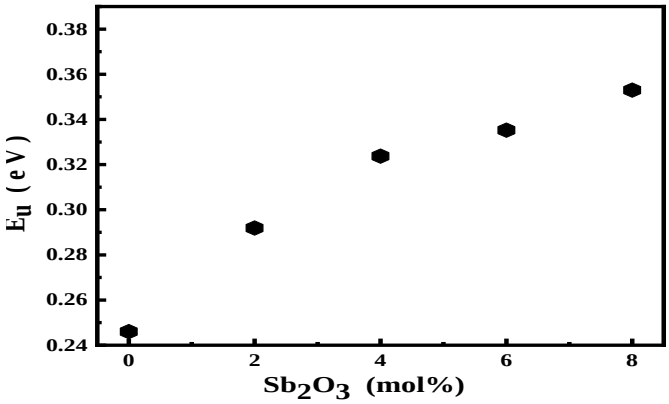

Fig. 7: E_u as a function of Sb_2O_3 (mol%) of the prepared glasses

3.4 Spectroscopic analysis of FTIR spectrum

The structural modifications that led to the observed changes in the physical characteristics of these glasses were investigated using infrared analysis. Figure (8) depicts the calculated Fourier transform. Transform infrared spectra of samples tested in the region of 4000 to 400 cm^{-1}, where each graphic reflects the relative absorption versus wavenumber of a single sample. There are no clear peaks of water absorption groups above 2000 cm^{-1}. As the presence of Sb_2O_3 in the sample increased from 0 to 8 mol%, the band that emerged at 1000 cm^{-1} shifted to around 980 cm^{-1}, and the band that formed at 700 cm^{-1} changed to around 680 cm^{-1}. These changes can be linked to the progressive increase of Sb_2O_3 concentration, which acts to enhance the non-bridging oxygen ions, as well as the glass network increasing ionic nature. Both aluminum and iron cations are thought to participate in the network of the examined glasses as (tetrahedral) groups, based on the FTIR data. This implies that both cations interact with the glass networks in the same way.

This might be due to the reduced proportion of SiO_2 (less than 50 mol percent). Ca^{2+}, Na^{+1}, and Mg^{2+} cations are thought to occupy only the glass network modifier locations. For phonon energy, the greatest intensity Sb–O–Sb stretching band is 602 cm^{-1} [5] while the other one at 1000-980 cm^{-1} is due to the B–O–B stretching vibration of the [BO_4] unit. The reflection band around 1300 cm^{-1} is due to the B–O–B stretching vibration of the [BO_3] unit[5]. In other words, none of the samples examined showed water adsorption, indicating that they might be used in a variety of applications this is due to these glasses not pure borate glasses, but all of the samples contained side by side B_2O_3. For x = 6, the region from 2000 to 400 cm^{-1} was chosen to de-convolute the FTIR master curve of each sample independently, as shown in figure (9). The de-convolution technique produced distinct peaks for each sample, with Wavenumbers, and FTIR spectra assignments are listed in table (2). The strength of these bands decreases as the antimony ion level rises. The significant absorption peak is due to the oscillation of the chemical link (Fe^{3+}–O^{-2}) in the octahedron's B position [20]. The intensity of this band increases as the antimony ions concentrations was increased.

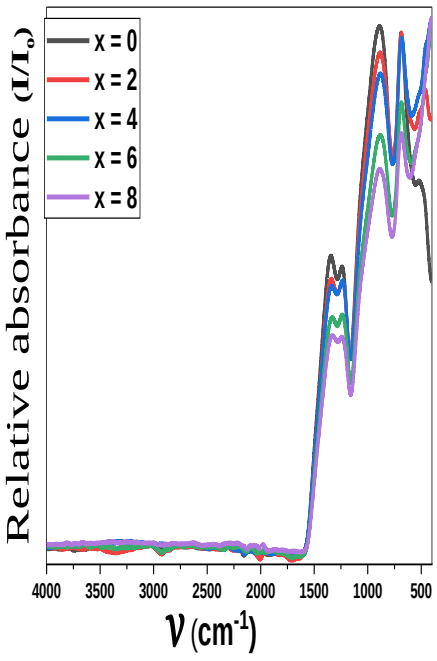

Fig. 8: FTIR spectra of the prepared glasses.

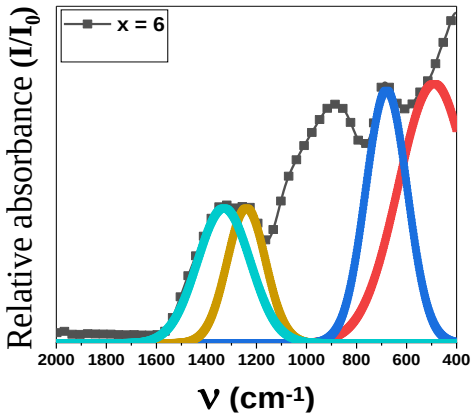

Fig. 9: De- convoluted FTIR spectrum of the prepared glass for x= 6 sample

4.5 Attenuation factors:

The slope of attenuation curves at photon energies of 80, 356, 662, 1173, and 1333 keV, obtained from ^{133}Ba, ^{137}Cs, and ^{60}Co γ-ray sources, respectively, were used to calculate the photon attenuation coefficients (μ) of the investigated samples. Using the values of and the observed densities of the samples, the mass attenuation coefficient μ_m (cm^2 /gm) was determined it. Fig. 10 shows the variation of μ_m values at different Sb_2O_3 concentration for photons of energy range from 80 MeV to 1333 keV. The values of μ_m increase with increasing Sb_2O_3 content, and decrease with increasing the energy of gamma photons. Because of the ~~many~~ partial interacting processes of a photon in different energy zones, such variation may be described by the photon energy emitted. Depending on the atomic number Z, the photoelectric reaction is dominant in the low-energy zone [23]. The greatest values reported for μ_m in the measurements energy areas may be explained by the same as seen of atomic number dependency. The principal interaction in the upper energy zone is Compton dispersion, which changes linearly with the atomic number. At high energies, the values of μ_m for all glass systems are almost equal, and the difference between μ_m values is zero.[23][24]. Higher μ_m values are desired for better materials as a radiation barrier. As a result, glass with a higher concentration of Sb_2O_3 is better for blocking the γ-ray. The HVL values that observed for all the glass samples increased with increasing photon energy, as seen in Fig.11. As a result, discrepancies in Z_{eff} values for produced glasses with different Sb_2O_3 and photon energy were direct repercussions of the mass attenuation results and the related HVL values. The MFP reflects the average distance traversed by particle motion between two consecutive interactions with other molecules. Fig. 12 demonstrates how MFP values change with Sb_2O_3 concentrations ranging from 662 keV to 1333 keV. MFP values lowered drop with

Table 2: Peak assignment of the prepared glasses:

Vibrational modes	**mber, (cm^{-1})**
Are accredited to Ca^{2+}, Na^{+1} and Mg^{2+} [21]	
Si-O-Si bending vibration Si-O-Al[22]**, The vibration of the chemical bond (Fe^{3+}–O^{2-}) in B location of the octahedron**[20]	;
Are due to bending vibrations of B–O linkages in the borate units[21]**, Si-O-Al stretching**[22]	
Are accredited to vibrations of tetrahedral BO_4 groups[21]**, Si-O-asymmetric stretching and Si-O-Al stretching** [22]	0
Si-O-Si asymmetric stretching[22]	
Are accredited to the stretches of B–O in BO_3 (or BO_2O^-) groups[20]	50

increasing Sb_2O_3 concentration and increase with increasing γ ray energy, suggesting that this glass has better shielding efficiency specialized for the high Sb_2O_3 content. Based on these findings, we consider that this glass might be used as a gamma ray shield if it contains an adequate content of Sb_2O_3. Figs. 13, 14 illustrate the behavior of all produced glasses with atomic cross sections σ_a and Z_{eff} in the energy range of 80 to 1333 keV interaction. For all created glasses containing Sb_2O_3, for a Compton interaction, and for pair formation, it is proportional to Z^2. When a result, as more Sb_2O_3 was added, the Z_{eff} values rose. The rise in Z_{eff} was attributable to the fact that the cross section of glass doped Sb is higher than that of undoped Sb. All samples show an increase in Z_{eff} as the incident photon energy increases in the low energy range $<$ 0.1 MeV, where photoelectric interactions are prevalent[24][25] .In all samples, the greatest Z_{eff} value was around 80 keV and the lowest Z_{eff} value was at 1333 keV. Figs. 15, 16 showed that the measured N_{eff} and Z_{eq} values for all the studied glasses at 80, 356, 662, 1173, and 1332 keV. Fig. 17 shows the computed fast neutron removal cross-section $\sum_R$ (cm^{-1}) values for the prepared glasses; the lowest $\sum_R$ value was achieved at Sb_2O_3 free sample, and the greatest at 8 mol% Sb_2O_3. The composite glass with the largest proportion of Sb ions had the highest neutron removal cross section, according to these findings. Low-Z elements may thus be responsible for neutron elimination, although a mixture of low-Z and intermediate-Z elements might accomplish comparable outcomes[23][23].

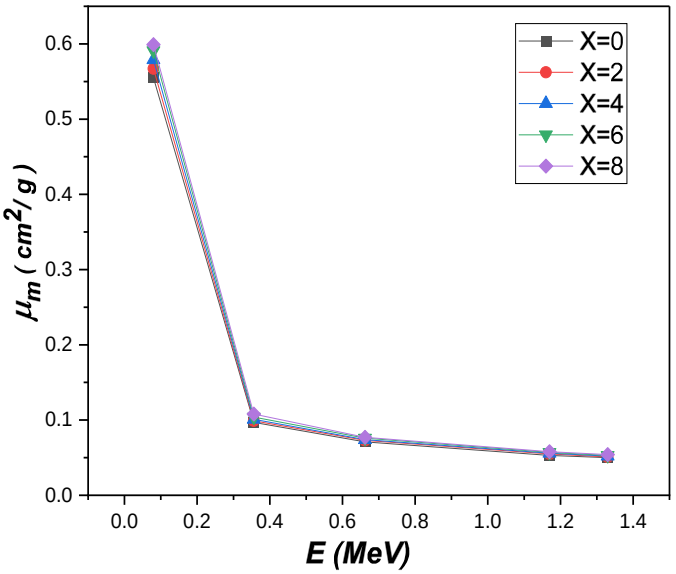

Fig. 10**:** Variation of mass attenuation coefficient (μ_m) with energy (E) for different Sb_2O_3 content.

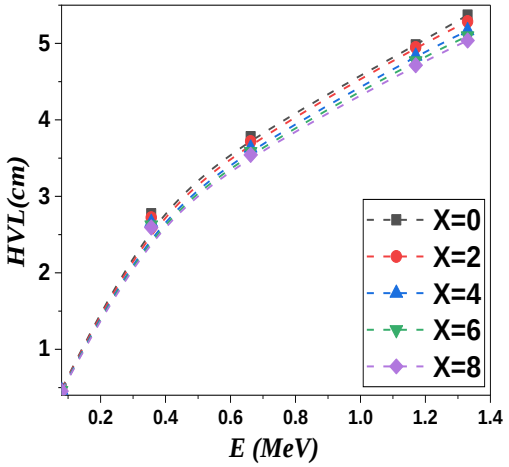

Fig. 11: Variation of half value layers (HVL) with photon energy (E) at different Sb_2O_3 content.

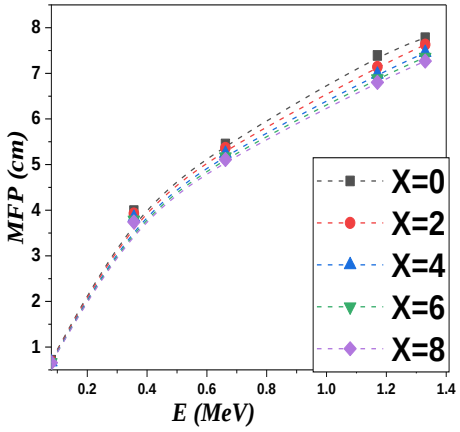

Fig. 12: Variation of mean free path MFP (λ) with photon energy (E) at different Sb_2O_3 content.

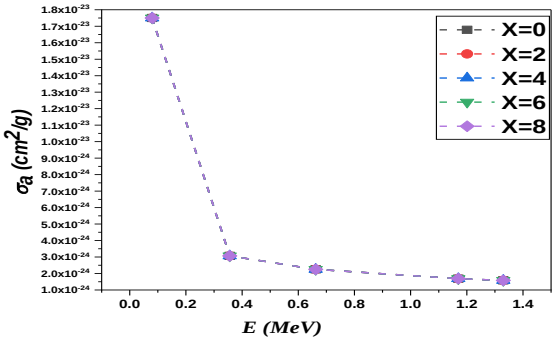

Fig. 13: Variation of atomic cross section σ_a with photon energy (E) at different Sb_2O_3 content.

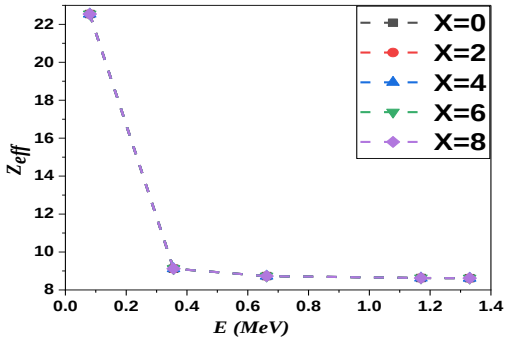

Fig.14: Variations of effective atomic number Z_{eff} with photon energy(E) at different Sb_2O_3 content

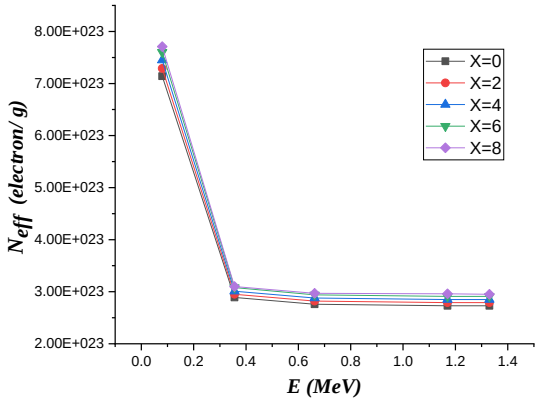

Fig. 15: Variations of effective electron density N_{eff} with photon energy (E) at different Sb_2O_3 content.

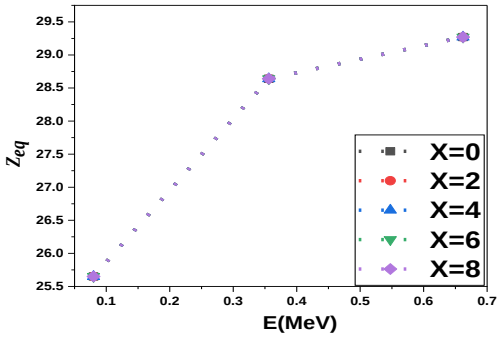

Fig. 16: Variation of equivalent atomic number (Z_{eq}) with photon energy (E) at different Sb_2O_3 content

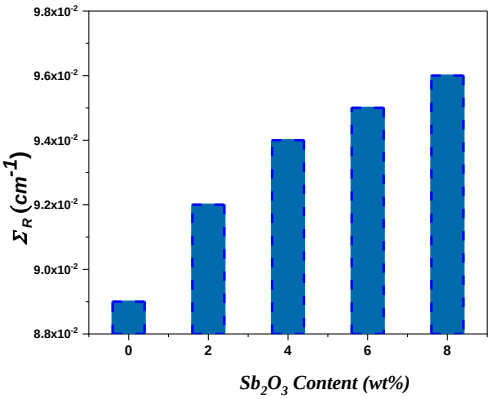

Fig. 17: Fast neutron removal cross sections $\sum_R$ (cm^{-1}) for borate glasses containing different concentrations of Sb_2O_3.

Conclusion:

The following conclusions may be extracted from this research:

1. The Sb_2O_3 concentration has a unique effect on density and molar volume. With a rise in Sb_2O_3

concentration, the density and molar volume increase.

2. The addition of Sb_2O_3 and the composition of Rock Wool result in a conversion from 3 to 4-fold coordinated boron, as determined by IR transmission spectra across a continuous spectral range (400–4000 cm^{-1}).

3. As the amount of Sb_2O_3 in the system grows, the optical bandgap decreased and the Urbach energy increased due to the increased of the presence of non-bridging oxygen.

4. The lowest energy had the greatest values of mass attenuation coefficients, whereas the highest energy had the highest half value layer.

5. For free Sb_2O_3, the largest effective atomic number was reached at 80 keV photon energy, whereas the minimum Z_{eff} for all glasses was found at 1333 keV photon energy.

6. As the Sb_2O_3 concentration of Rock Wool borate glasses increase, all radiation shielding properties improved.

References:

[1] R. Limited and N. Court, "RockShield External Wall Insulation System," vol. 7, no. 10, pp. 1–23, 2017.

[2] J. Diekmann and C. Hanisch, "New circular building composite material to upcycle building wastes New circular building composite material to upcycle building wastes," 2021, doi: 10.1088/1742-6596/2042/1/012167.

[3] X. Li *et al.*, "Simulating Study on Mechanical Properties of Rock Wool Board for Thermal Insulation on External Walls," vol. 2020, 2020.

[4] V. Dimitrov and T. Komatsu, "Average single bond strength and optical basicity of Bi2O3-B2O3 and Sb2O3-B2O3 glasses," *J. Non. Cryst. Solids*, vol. 356, no. 4–5, pp. 258–262, 2010, doi: 10.1016/j.jnoncrysol.2009.11.014.

[5] T. Som and B. Karmakar, "Optical properties of Eu3+-doped antimony-oxide-based low phonon disordered matrices," *J. Phys. Condens. Matter*, vol. 22, no. 3, 2010, doi: 10.1088/0953-8984/22/3/035603.

[6] T. Satyanarayana *et al.*, "Structural investigations on PbO-Sb2O3-B 2O3:CoO glass ceramics by means of spectroscopic and dielectric studies," *J. Phys. Condens. Matter*, vol. 21, no. 24, 2009, doi: 10.1088/0953-8984/21/24/245104.

[7] M. Erdem, O. Baykara, M. Doğru, and F. Kuluöztürk, "A novel shielding material prepared from solid waste containing lead for gamma ray," *Radiat. Phys. Chem.*, vol. 79, no. 9, pp. 917–922, 2010.

[8] F. A. Gaber, M. A. El-Sarraf, and W. A. Kansouh, "Utilization of boron oxide glass and epoxy/ilmenite assembly as two layer shield," *Ann. Nucl. Energy*, vol. 57, pp. 106–110, 2013.

[9] A. M. Reda and A. A. El-Daly, "Gamma ray shielding characteristics of Sn-20Bi and Sn-20Bi-0.4 Cu lead-free alloys," *Prog. Nucl. Energy*, vol. 123, p. 103304, 2020.

[10] S. A. El-Gharbawy *et al.*, "Fabrication and Characterization of Nanostructured Rock Wool as a Novel Material for Efficient Water-Splitting Application," *Nanomaterials*, vol. 12, no. 13, p. 2169, 2022, doi: 10.3390/nano12132169.

[11] H. Doweidar, G. M. El-Damrawi, Y. M. Moustafa, and R. M. Ramadan, "Density of mixed alkali borate glasses: A structural analysis," *Phys. B Condens. Matter*, vol. 362, no. 1–4, pp. 123–132, 2005, doi: 10.1016/j.physb.2005.02.001.

[12] J. S. Dhillon, B. Singh, and G. S. Sidhu, "A comprehensive study on energy absorption and exposure buildup factors for some Vitamins and Tissue," vol. 2, no. 9, pp. 1–8, 2012.

[13] M. Milling, M. Cengiz, H. Oh, and H. Lee, "Neutron / gamma radiation shielding characteristics Neutron / gamma radiation shielding characteristics and physical properties of (97 . 3 − x) Pb − xCd − 2 . 7Ag alloys for nuclear radiation applications".

[14] S. M. S. and A. G. M. A.M. Abdel-Ghany , M.S.S. Saad , I.I. Bashter , T.Z. Amer, "Studies on Some Inorganic Oxide Glasses Used as Gamma-Ray Shields and for Radio-Active Waste Encapsulationtle," *Nat. Sci.*, vol. 12, no. 12, pp. 162–170, 2014.

[15] A. M. El-Khayatt and H. A. Saudy, "Preparation and characterization of zinc, lanthanum white sand glass for use in nuclear applications," *Radiat. Phys. Chem.*, vol. 166, no. September 2019, p. 108497, 2020, doi: 10.1016/j.radphyschem.2019.108497.

[16] V. Bhatia, D. Kumar, A. Kaur, D. Singh, A. Singh, and S. P. Singh, "Investigation of optical and physical properties of zinc sodium bismuth borate glass system," *IOP Conf. Ser. Mater. Sci. Eng.*, vol. 1033, no. 1, 2021, doi: 10.1088/1757-899X/1033/1/012073.

[17] H. A. Saudi and S. U. El-Kameesy, "Investigation of modified zinc borate glasses doped with BaO as a nuclear radiation-shielding material," *Radiat. Detect. Technol. Methods*, Nov. 2018, doi: 10.1007/s41605-018-0075-x.

[18] E. S. Yousef, M. M. Elokr, and Y. M. Aboudeif, "Optical, elastic properties and DTA of TNZP host tellurite glasses doped with Er3+ ions," *J. Mol. Struct.*, vol. 1108, 2016, doi: 10.1016/j.molstruc.2015.11.066.

[19] S. M. Kamil, A. A. Abul-Magd, W. El-Gammal, and H. A. Saudi, "Enhanced optical and structural features of Ni2+/La3+ hybrid borate glasses," *Spectrochim. Acta Part A Mol. Biomol. Spectrosc.*, no. xxxx, p. 120569, 2021, doi: 10.1016/j.saa.2021.120569.

[20] P. Pascuta, G. Borodi, M. Bosca, L. Pop, S. Rada, and E. Culea, "Preparation and structural characterization of some Fe2O 3-B2O3-ZnO glasses and glass ceramics," *J. Phys. Conf. Ser.*, vol. 182, no.

1, pp. 3–7, 2009, doi: 10.1088/1742-6596/182/1/012072.
[21] A. F. Abd El-Rehim and K. S. Shaaban, “Influence of La 2 O 3 content on the structural, mechanical, and radiation-shielding properties of sodium fluoro lead barium borate glasses”, doi: 10.1007/s10854-020-05204-7.
[22] J. Xie, Z. F. Xiao, W. H. Zheng, Y. Liu, and J. S. Cheng, “The Effect of Al_2O_3/SiO_2 on the Structure and Properties of Na_2O-CaO-Al_2O_3-SiO_2 Glasses,” *Key Eng. Mater.*, vol. 509, pp. 339–345, 2012, doi: 10.4028/www.scientific.net/kem.509.339.
[23] H. C. Manjunatha, L. Seenappa, C. B.M, K. N. Sridhar, and C. Hanumantharayappa, “Gamma, X-ray and neutron shielding parameters for the Al-based glassy alloys,” *Appl. Radiat. Isot.*, 2018, doi: 10.1016/j.apradiso.2018.05.014.
[24] P. Sikora, A. M. El-Khayatt, H. A. Saudi, S. Y. Chung, D. Stephan, and M. Abd Elrahman, “Evaluation of the effects of bismuth oxide (Bi2O3) micro and nanoparticles on the mechanical, microstructural and γ-ray/neutron shielding properties of Portland cement pastes,” *Constr. Build. Mater.*, vol. 284, p. 122758, 2021, doi: 10.1016/j.conbuildmat.2021.122758.
[25] I. S. Mahmoud *et al.*, “Material characterization of WO3/Bi2O3 substituted calcium-borosilicate glasses: Structural, physical, mechanical properties and gamma-ray resistance competencies,” *J. Alloys Compd.*, vol. 888, p. 161419, 2021, doi: 10.1016/j.jallcom.2021.161419.
[26] H. M. Gomaa, H. A. Saudi, I. S. Yahia, M. A. Ibrahim, and H. Y. Zahran, “Influence of exchanging CeO2 with Cu2O3 on both structural matrix, shielding, and linear/nonlinear optical parameters of the cerium-sodium borate glass,” *Optik (Stuttg).*, p. 168267, 2021, doi: 10.1016/j.ijleo.2021.168267.
[27] A. M. El-Batal, M. A. Farag, M. M. El-Okr, and A. Saeed, “Influence of the Addition of Two Transition Metal Ions to Sodium Zinc Borophosphate Glasses for Optical Applications,” *Egypt. J. Chem.*, vol. 64, no. 12, pp. 6953–6958, 2021, doi: 10.21608/EJCHEM.2021.79765.3921.
[28] M. A. Farag, A. Ibrahim, M. Y. Hassaan, and R. M. Ramadan, “Enhancement of structural and optical properties of transparent sodium zinc phosphate glass–ceramics nano composite,” *J. Aust. Ceram. Soc.*, vol. 58, no. 2, pp. 653–661, 2022, doi: 10.1007/s41779-022-00716-3.